nature water

Article

https://doi.org/10.1038/s44221-024-00326-2

Spontaneous lithium extraction and enrichment from brine with net energy output driven by counter-ion gradients

Received: 16 May 2024

Accepted: 25 September 2024

Published online: 24 October 2024

Check for updates

Ge Zhang[1], Yuqi Li[1], Xun Guan[1], Guoliang Hu[1], Hance Su[1], Xueer Xu[1], Guangxia Feng[1], Sanzeeda Baig Shuchi[2], Sang Cheol Kim[1], Jiawei Zhou[1], Rong Xu[1], Xin Xiao[1], Allen Wu[1] & Yi Cui[1,3]

To meet the increasing lithium demands created by global electrification, a fast, flexible, inexpensive and sustainable mining process is needed, which is yet to be realized. Here we explore an untapped energy source that is inherent in all ion-separation processes to achieve spontaneous Li extraction with net energy production. The driving force comes from the huge concentration difference of counter ions (usually chloride) between the feeding and receiving solutions. Experimental results under various feeding compositions can be well explained by the Gibbs–Donnan equilibrium. Utilizing a Li-selective ceramic membrane and a chloride-storing silver electrode, we successfully achieved Li extraction from simulated brine with an energy output of 1.6 Wh mol_{Li}^{-1}. The system is stable over 300 hours of operation, maintaining a high Li/Mg selectivity of 450. Moreover, even spontaneous enrichment can be achieved when the counter ion concentration is much greater than that of Li ion in the feeding brine. We anticipate that the concept of this work could not only reshape the Li supply chain but also seed a fundamental transformation of all ion-separation processes.

The global production of Li has more than tripled during the past decade, driven by the rapid growth of renewable energy storage and the electric vehicle market[1,2]. Various studies have predicted that the demand for Li will triple again in the coming decade[3,4]. Currently, global Li production is dominated by evaporation-driven mining from continental brines, followed by chemical precipitation from minerals[5–8]. However, none of these traditional techniques provide a satisfying solution to the ever-increasing Li demands. The evaporation process is extremely slow, making Li production inflexible and hard to respond to short-term changes in market demand[7]. Even with novel device structures and materials[9–11], evaporation-based methods still waste large amounts of water, which not only limits their energy efficiency but also induces damage to the environment[12]. In addition, such methods are typically not suitable for resources with lower Li content, such as oil-produced water and geothermal brines[4,13].

In recent years, direct Li extraction techniques have emerged as promising alternatives to traditional techniques due to their higher efficiency, lower capital investment, better production flexibility and environmental compatibility[14,15]. Ion pumping processes, especially electrochemical Li extraction, have received a lot of attention in recent years[16–19]. Intercalation cathodes with inherent preference for Li over other cations, such as $LiCoO_2$[20], $LiFePO_4$[21–23] and $LiMn_2O_4$[24–26], ensure the high selectivity of ion pumping processes. Nonetheless, these techniques have limited throughput because of necessary post-treatment

[1]Department of Materials Science and Engineering, Stanford University, Stanford, CA, USA. [2]Department of Chemical Engineering, Stanford University, Stanford, CA, USA. [3]Stanford Institute for Materials and Energy Sciences, SLAC National Accelerator Laboratory, Menlo Park, CA, USA.
e-mail: yicui@stanford.edu

https://doi.org/10.1038/s44221-024-00326-2

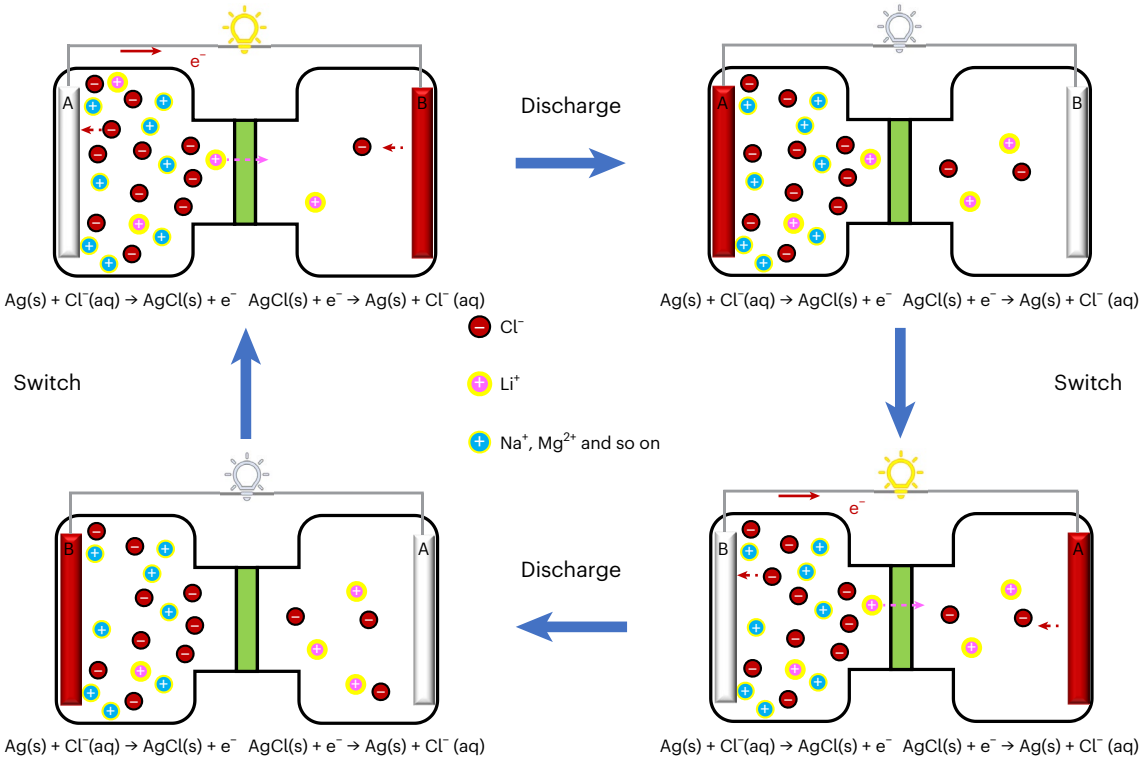

Fig. 1 | Concept. Spontaneous Li extraction and enrichment with net energy output can be achieved using a Li-selective membrane with a pair of Ag/AgCl electrodes. Repeatedly switching the Ag and AgCl electrodes enables semi-continuous Li extraction.

steps to regenerate the adsorbent and low current density to prevent co-intercalation of impurities.

Membrane-based techniques such as electrodialysis, electrolysis and nanofiltration offer many advantages over other direct Li extraction methods, such as lower chemical emission, higher selectivity and continuous operation[27,28]. Although nanofiltration features an outstanding rate and low energy cost, it often suffers from poor selectivity towards Li as a result of insufficient pore size control. Li/Na separation is particularly difficult because they cannot be distinguished by charge density like Li/Mg separation[29–40]. To make things worse, hydrated Li^+ actually has a larger radius than Na^+, making most nanofiltration membranes prefer Na over Li[41–45]. Fortunately, effective Li/Na separation can be realized by solid Li electrolytes, which can fully dehydrate Li^+ and Na^+ (making Li^+ smaller than Na^+). Since the first attempt by Itoh and co-workers in 1999[46], various types of solid Li electrolyte, including NASICON-type $Li_{1.5}Al_{0.5}Ge_{1.5}(PO_4)_3$ (LAGP)[47–52] or $Li_{1.5}Al_{0.5}Ti_{1.5}(PO_4)_3$ (LATP)[53–56], garnet-type $Li_{6.4}La_3Zr_{1.4}Ta_{0.6}O_{12}$ (LLZTO)[57–63] and perovskite-type $Li_{0.33}La_{0.56}TiO_3$ (LLTO)[46,64–68], have been employed for electrodialytic or electrolytic Li extraction. Hoshino[64] and Lai and co-workers[66] used ceramic membranes to extract Li ion from seawater, whereas Zhou and co-workers[61] further developed an electrolysis process to produce metallic lithium from seawater. Despite the good selectivity and Faradaic efficiency, these processes employed the water-splitting reaction or chlor-alkali process to drive the migration of Li, both of which are plagued by high thermodynamic potentials and overpotentials[49,64,66]. As a consequence, these devices usually operate at high voltages greater than 3 V, severely increasing their energy consumption. He, Lai and Huang and co-workers[50,52] integrated photoelectrodes with Li extraction devices to utilize solar energy, but the delicate semiconductor structure introduced additional challenges for fabrication. Very recently, two works by Cui and co-workers[69] and Presser and co-workers[70] have dramatically reduced the operation voltage to below 1 V by introducing reversible redox couples (hydrogen reduction/oxidation, ferri/ferrocyanide redox) across the two electrodes[69,70].

In this Article, we leverage an untapped driving force embedded in ion-separation processes, which not only eliminates the energy cost of electrodialytic Li extraction but can even produce energy. The critical improvement is finding an electrode reaction to exploit the tremendous osmotic energy, which is a result of the huge concentration difference of counter ions between the feeding and receiving solutions. A thermodynamic model based on the Gibbs–Donnan effect is established to describe the driving force quantitatively, which matches well with experimental results. Practically, spontaneous Li extraction with an energy output of 1.6 Wh mol_{Li}^{-1} is demonstrated using an LAGP membrane and a pair of Ag/AgCl electrodes. A high Li/Mg selectivity of 450 can be maintained for 300 h, with close-to-unity Faradaic efficiency. Furthermore, even spontaneous enrichment is feasible as indicated by both theory and experiments. This work essentially combines the Li extraction process with osmotic energy harvesting into one device, breaking the conventional thinking that ion separation and enrichment should be energy consuming. We expect that the concept and general principle of this work is applicable to more ion-separation processes and can potentially inspire a new field of carbon-negative resource extraction.

Results

Concept of spontaneous Li extraction

The working principle of spontaneous Li extraction is illustrated schematically in Fig. 1. A piece of Li-selective membrane separates the pure LiCl receiving solution from the feeding brine, which contains large amounts of other cations (Na^+, Mg^{2+} and so on). When a pair of Ag and AgCl electrodes are placed into the feeding and receiving chambers, respectively, an electrochemical potential will be generated due to the concentration difference of ions in the two chambers. Such a potential can drive Li^+ through the single-ion conductive membrane, whereas Cl^- is incorporated into or released out of the Ag/AgCl electrodes. After being fully discharged, the Ag and AgCl electrodes can be switched and the device is able to discharge again, hence achieving semi-continuous Li extraction.

https://doi.org/10.1038/s44221-024-00326-2

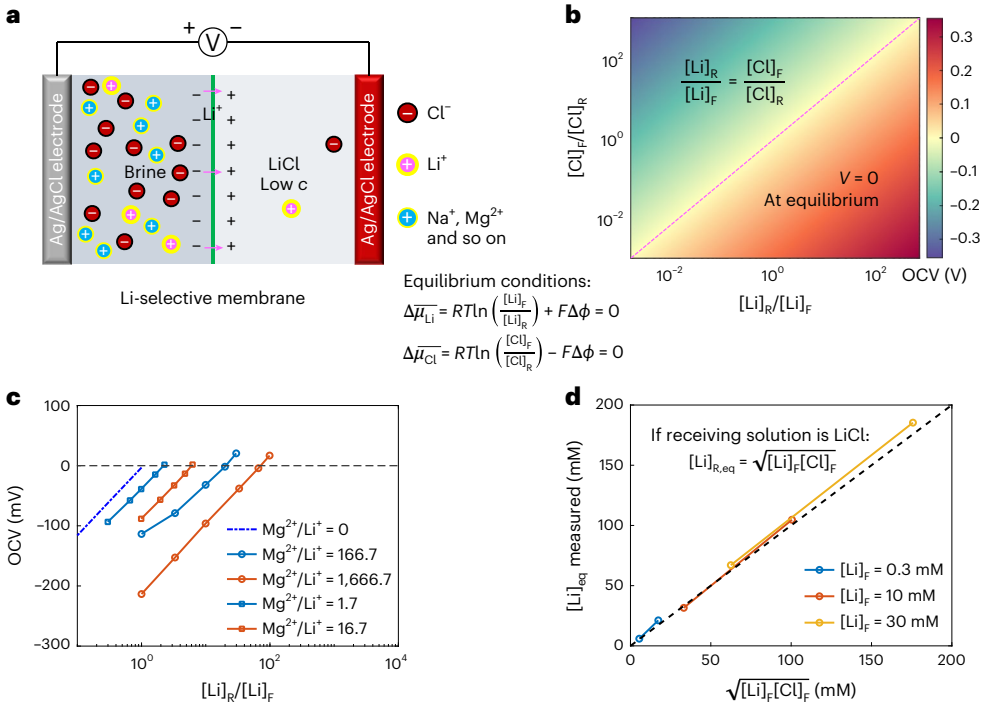

Fig. 2 | Equilibrium conditions of Li extraction processes. a, Schematics of a spontaneous Li extraction cell at open circuit condition. **b**, Heat map of OCV as a function of Li^+ and Cl^- concentration ratios across the membrane. The equilibrium condition of $\frac{[Li]_F}{[Li]_R} = \frac{[Cl]_R}{[Cl]_F}$ can be derived by matching the electrochemical potential of Cl^- and Li^+ across the membrane. F, feeding; R, receiving. **c**, Experimental OCV versus Li^+ concentration ratio across the membrane at various Mg/Li ratios in the feeding solution. The blue dashed curve represents pure LiCl as the feeding solution. The blue solid curves have 50 mM of $MgCl_2$, whereas the red curves have 0.5 M $MgCl_2$ in the feeding solution. The concentration of LiCl in the feeding solution is 0.3 mM and 30 mM for the curves with round and square symbols, respectively. **d**, Comparison of equilibrium concentration of Li^+ measured by experiment in **c** versus predicted by theory in **b**. For each feeding LiCl concentration, we have tested 2 feeding $MgCl_2$ concentrations: 50 mM and 500 mM. The lower points for each feeding LiCl concentration correspond to 50 mM $MgCl_2$ concentration, and the higher ones correspond to 500 mM.

The thermodynamic driving force of this system purely comes from concentration difference, in another word, osmotic energy. However, the blocking of all cations other than Li^+ creates an imbalance of osmotic pressure for anions and cations. The much larger osmotic pressure of Cl^- due to its higher concentration in brine than Li^+ provides ample driving force for Li^+ that can even achieve Li enrichment.

To understand the driving force quantitatively, let's first consider the open circuit voltage (OCV) of a spontaneous Li extraction cell (Fig. 2a), which is the sum of the membrane potential difference $\Delta\phi_m$ and the electrode potential difference $\Delta\phi_N$.

$$\mathrm{OCV} = \Delta\phi_m + \Delta\phi_N \tag{1}$$

With Ag/AgCl electrodes, $\Delta\phi_N$, which represents the osmotic energy from Cl^-, can be easily determined using the Nernst equation, where R is the ideal gas constant, T is the temperature, F is the Faradaic constant, and $[Cl]_F$ and $[Cl]_R$ are the concentrations of Cl^- in the feeding and receiving solutions:

$$\Delta\phi_N = -\frac{RT}{F}\ln\left(\frac{[Cl]_F}{[Cl]_R}\right) \tag{2}$$

The membrane potential $\Delta\phi_m$ can be determined by considering the equilibrium condition for Li across the membrane. When brine and receiving solution get in contact with a Li-selective membrane, a tiny amount of Li^+ will diffuse towards the side with lower concentration, breaking charge neutrality in the vicinity of the membrane surface (Fig. 2a). The resulting electric field acts against the concentration gradient of Li^+ to stop its further diffusion, which requires the electrochemical potential of Li^+ to be equal on both sides of the membrane. Assuming both solutions are ideal, all salts fully dissociate and the activity of each ion is the same as its concentration, we have the following condition for equilibrium at open circuit:

$$\Delta\overline{\mu_{Li}} = RT\ln\left(\frac{[Li]_F}{[Li]_R}\right) + F\Delta\phi_m = 0 \tag{3}$$

$$\Delta\phi_m = -\frac{RT}{F}\ln\left(\frac{[Li]_F}{[Li]_R}\right) \tag{4}$$

Hence the open circuit voltage is:

$$\mathrm{OCV} = -\frac{RT}{F}\left[\ln\left(\frac{[Li]_F}{[Li]_R}\right) + \ln\left(\frac{[Cl]_F}{[Cl]_R}\right)\right] \tag{5}$$

Here $\Delta\phi_m = \phi_F - \phi_R$ is the electrostatic potential drop across the membrane, and $[Li]_F$, $[Li]_R$, $[Cl]_F$ and $[Cl]_R$ are the concentrations of Li^+ and Cl^- in the feeding and receiving solutions, respectively. Anion concentration gradient clearly contributes more to the total driving force because typically $[Cl]_F \gg [Li]_F$ whereas $[Cl]_R = [Li]_R$. Because both Li^+ and Cl^- have higher concentrations in the brine, the OCV is negative based on the sign convention in Fig. 2a.

When the external circuit is closed, electrons will flow from the left Ag electrode (feeding) to the right AgCl electrode (receiving), which has higher electric potential, accompanied by Cl^- intake/release on the left/right electrode. The spontaneous flow of electrons towards a positive electrode infers energy generation. This weakens $\Delta\phi_m$, allowing continuous Li^+ flow through the membrane to balance the charge

https://doi.org/10.1038/s44221-024-00326-2

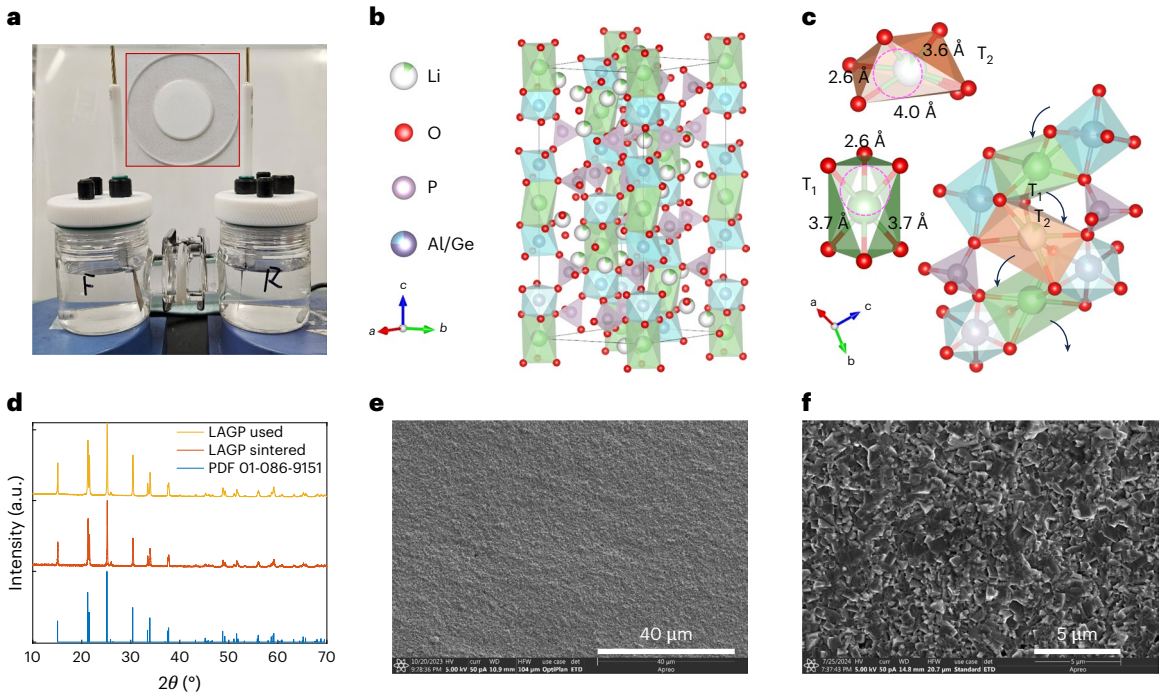

Fig. 3 | Structural characterization of LAGP membranes. a, Photographs of an H cell for spontaneous Li extraction. Inset: photo of an LAGP membrane fixed onto a plastic holder. **b**, Schematic of the crystal structure of $Li_{1.5}Al_{0.5}Ge_{1.5}(PO_4)_3$. **c**, Transport channels of Li+ in the LAGP structure with size information of the triangular bottlenecks. T_1 and T_2 represent the triangular bottlenecks in the Li diffusion pathways. **d**, XRD patterns of a sintered LAGP membrane before and after Li/Mg separation experiments. **e**, SEM image of the top surface of an LAGP membrane. **f**, SEM image of the cross section of an LAGP membrane.

of Cl^-. Overall, LiCl migrates towards the receiving solution, getting separated from other salts in the brine.

As more LiCl gets extracted, the driving force diminishes until OCV becomes 0 according to equation (5). The system now reaches the final equilibrium state satisfying the following condition:

$$\frac{[Li]_R}{[Li]_F} = \frac{[Cl]_F}{[Cl]_R} \tag{6}$$

On the basis of equation (6), equilibrium can only be achieved on the diagonal line in Fig. 2b where both Li^+ and Cl^- have equal electrochemical potential across the membrane. The theory has been proposed by Gibbs and Donnan over a century ago but has not seen applications in Li extraction yet[71].

To verify the above theory, experimental measurements of the OCV have been carried out, and the results are summarized in Supplementary Fig. 1. In each set of experiments, the composition of the feeding solution is fixed whereas the concentration of LiCl in the receiving solution is increased gradually. Figure 2c shows the average OCV as a function of the concentration ratio of Li^+ across the membrane. As predicted by equation (5), the OCV is more negative when the ratio of $\frac{[Li]_F}{[Li]_R}$ and $\frac{[Cl]_F}{[Cl]_R}$ are larger. The curves move to the right as the ratio of Mg^{2+} (hence Cl^- as well) to Li^+ gets larger, which is also expected according to equation (5). On a semi-log plot such as Fig. 2c, the slope of the curves is expected to be 118 mV per decade (10-fold change in the concentration) at room temperature because $[Li]_R = [Cl]_R$:

$$OCV = \frac{RT}{F}\ln(10)\log\left([Li]_R[Cl]_R\right) + C \tag{7}$$

The experimental values of the slope range from 100 to 120 mV per decade, which qualitatively matches the theory and substantially exceeds the slope based on the Nernst equation of a single species. The small deviation could be due to some non-ideality of the Li-conductive membrane and the electrodes. For example, Li^+ in the membrane may undergo slow exchange with proton in water if Li^+ concentration is very low in solution[72], whereas surface complexation of AgCl with excessive Cl^- in the solution may cause a lower slope than predicted by Nernst equation[73]. The constant C in equation (7) is related to the concentration of Cl^- and Li^+ in the feeding solution hence it is fixed in the experiments above.

The interception points of these curves with the line of OCV = 0 give the equilibrium composition of the receiving solutions under different feeding conditions. When the receiving solution contains only LiCl, $[Li]_R = [Cl]_R$ and the equilibrium condition in equation (6) can be further simplified to:

$$[Li]_{R,eq} = \sqrt{[Li]_F[Cl]_F} \tag{8}$$

This conclusion is validated by the results as shown in Fig. 2d, where the experimentally measured equilibrium concentration of Li matches closely with the prediction by equation (8).

Overall, the experimental results and the theory both demonstrate that a substantial amount of energy can be extracted when Li^+ is separated from other cations in the brine. Furthermore, the thermodynamic driving force is strong enough to even enable spontaneous Li enrichment without any energy input. In the theoretical limit, our approach can enable a 14.2-fold or 44.7-fold enrichment when the molar ratio of Mg to Li is 100 or 1,000 in the brine, respectively.

Demonstration of spontaneous Li extraction and enrichment

The experimental set-up for spontaneous Li extraction is shown in Fig. 3a. The critical component for achieving spontaneous Li extraction is a highly selective membrane (Fig. 3a, inset). To achieve the highest possible extraction performance, NASICON-type LAGP ($Li_{1.5}Al_{0.5}Ge_{1.5}(PO_4)_3$) is chosen in this work due to its high Li conductivity[74]

https://doi.org/10.1038/s44221-024-00326-2

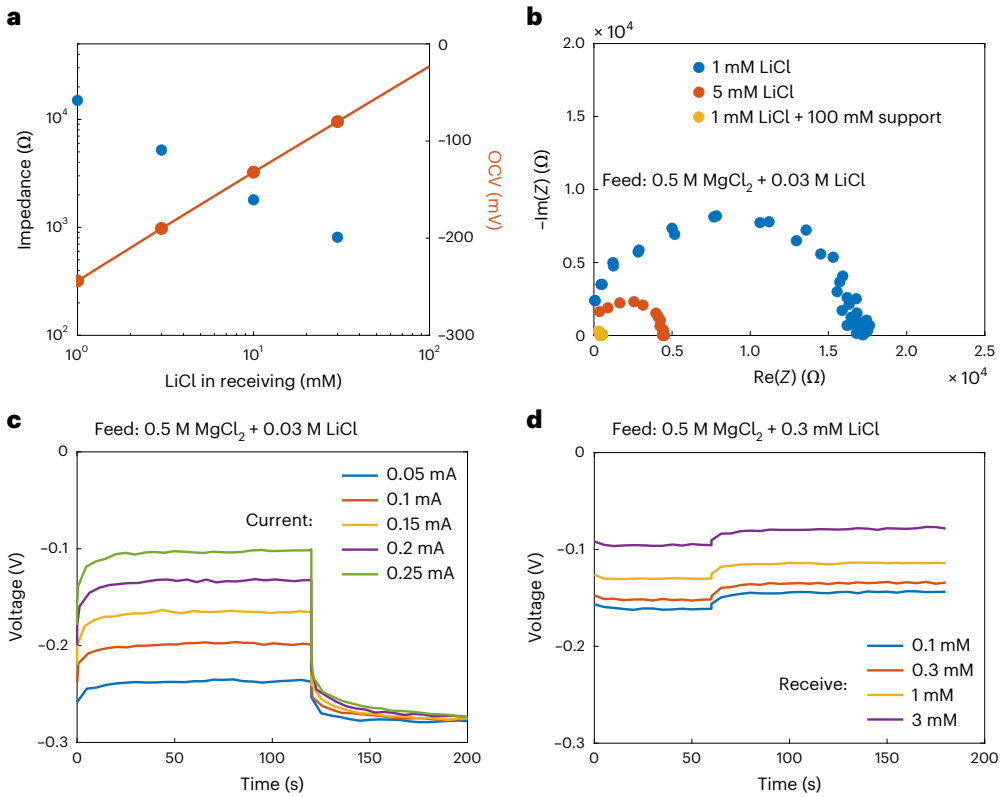

Fig. 4 | Proof of concept demonstration. a, OCV and cell impedance results versus LiCl concentration in the receiving solution using 0.5 M $MgCl_2$ + 0.03 M LiCl as the feed, showing a dilemma between reducing impedance and increasing voltage. **b**, EIS spectra of cells with and without NH_4HCO_3 supporting electrolyte in the receiving solution, using 0.5 M $MgCl_2$ + 0.03 M LiCl as the feed. The impedance–voltage dilemma is solved by using the supporting electrolyte. Im(*Z*) and Re(*Z*) represent the imaginary and real parts of the cell impedance. **c**, Voltage curves under various current densities using 0.5 M $MgCl_2$ + 0.03 M LiCl as the feeding and 0.1 M NH_4HCO_3 as the receiving. The current is turned off after 120 s. **d**, Voltage curves under 10 μA current using 0.5 M $MgCl_2$ + 0.3 mM LiCl as the feeding and 0.1 M NH_4HCO_3 + 0.1 to 3 mM LiCl as the receiving. The current is turned on at 60 s. This demonstrates that spontaneous Li enrichment is possible.

and selectivity[75] at room temperature. Details of the preparation and characterization procedures have been elaborated in Methods and by previous works.

The LAGP crystal structure shown in Fig. 3b has a negatively charged backbone, composed of corner and edge sharing Al–O, Ge–O and P–O polyhedra. Li^+ partially occupies the Wyckoff sites 6*b*, 18*e* and 36*f*[49,51,76]. During the ionic transport, Li^+ has to pass through two triangular bottlenecks, whose inscribed circles are less than 1.8 Å in diameter (Fig. 3c). Na^+ (1.9 Å diameter) will encounter much larger energy barrier than Li^+ (1.2 Å diameter) when moving through these small channels[77]. Whereas Mg^{2+} possesses similar dehydrated ionic radii as Li^+, it has nearly four times larger (de)hydration free energy, which effectively blocks it from entering the LAGP crystal[78]. As a result, only small, dehydrated Li^+ cations are able to move through the crystal structure. The X-ray diffraction (XRD) pattern of sintered LAGP pellets is consistent with the standard pattern of $Li_{1.5}Al_{0.5}Ge_{1.5}(PO_4)_3$ (Fig. 3d). The crystal structure of the LAGP membrane remains unchanged even after prolonged operation for 300 h in Li/Mg separation experiment (Fig. 3d), confirming its excellent stability in aqueous solutions. Scanning electron microscopy (SEM) images of the top surface (Fig. 3e) and the cross section (Fig. 3f) of LAGP membrane both show a dense structure with closely packed grains. Overall, the dense and crack-free LAGP membrane prevents the crossover of water and any ions except Li^+, ensuring high selectivity for the extraction process.

Ag/AgCl electrode is selected as the driving electrode and Cl^- carrier for our experiments due to its stable electrode potential, small overpotential, ease of fabrication and absence of hazardous materials. The overall electrode reaction is:

$$AgCl(s) + e^- \rightleftharpoons Ag(s) + Cl^-(aq)$$

As oxidation occurs, the silver atom loses an electron and dissolves away from defect sites. Due to the low solubility of AgCl, it will gradually precipitate on the surface of silver metal to form a porous film, ranging from hundreds of nanometres to tens of micrometres in thickness[79]. Such a process probably goes through some soluble intermediate species such as $AgCl_2^-$, which can diffuse away from Ag dissolution sites and re-deposit at a different location[80]. As the AgCl layer grows, chloride ions are stored in a solid form on the electrode. In the receiving solution, reduction of AgCl goes through the reverse process as oxidation and releases the stored chloride. Loading silver particles onto a porous C paper substrate provides a larger surface area for AgCl deposition, compared to a planar metal surface. This could help to reduce the transport resistance and prevent AgCl passivation after repeated cycling.

To achieve spontaneous Li extraction in practice, a finite amount of current needs to be applied to the device. Therefore, it is important to reduce the internal resistance of the cell to minimize resistance loss and maximize energy output. The total resistance consists of several parts, including the charge-transfer resistance of the electrodes, the electrolyte resistance of the feeding and the receiving solution, and the resistance of the Li-selective membrane. Electrochemical impedance spectroscopy (EIS) reveals that the total resistance is dominated by the resistance of the receiving solution in most cases, due to its low concentration (Supplementary Fig. 2). At 1 mM concentration, the overall resistance of the cell exceeds 15,000 Ω, which prevents Li extraction at any meaningful rates. Increasing the LiCl concentration

https://doi.org/10.1038/s44221-024-00326-2

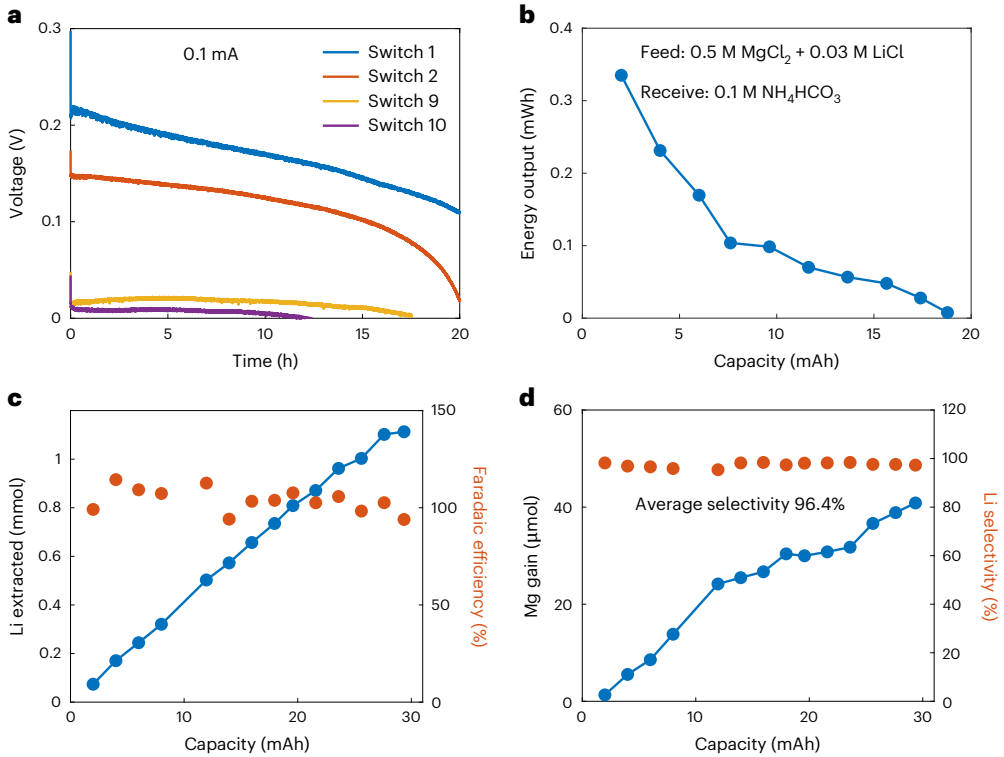

Fig. 5 | Long-term stability of spontaneous Li/Mg separation with energy output. a, Voltage curves under 0.1 mA current using 0.5 M $MgCl_2$ + 0.03 M LiCl as the feeding and 0.1 M NH_4HCO_3 as the receiving. The pair of electrodes has been switched ten times. Note that the sign of the voltage has been flipped in this particular figure. **b**, Energy versus capacity curve, showing that the output energy diminishes as the concentration gradient across the membrane decreases. **c**, Amount of Li extracted and Faradaic efficiency versus capacity. **d**, Amount of Mg leakage to the receiving side and Li selectivity versus capacity.

in the receiving solution by 100 times could lower the resistance to less than 500 Ω (Fig. 4a). However, this comes with the cost of a diminished driving force, reducing the OCV to only 23 mV as shown in Fig. 4a and Supplementary Fig. 2a.

Introducing a supporting electrolyte helps to resolve the dilemma between a high resistance and a low OCV. As demonstrated in Fig. 4b, the impedance of the cell is reduced by nearly two orders of magnitude after adding 100 mM of NH_4HCO_3 into the receiving solution. Meanwhile, the driving force will not be sacrificed because a very low concentration of LiCl can be used on the receiving side (Supplementary Fig. 3).

Galvanostatic discharge tests have been carried out to explore the feasibility of extracting energy from spontaneous Li extraction with the help of a supporting electrolyte. With 0.5 M $MgCl_2$ + 0.03 M LiCl as the feeding and pure 0.1 M NH_4HCO_3 as the receiving solution, the cell delivers an OCV of −0.25 V. Figure 4c proves that such a condition can produce net energy output with a notable voltage ($|U| \geq 0.1$ V) up to a current density of 0.25 mA cm^{-2} (based on the area of the membrane). The maximum power density of 0.028 mW cm^{-2} occurs at a current density of 0.2 mA cm^{-2} as Supplementary Fig. 4a shows. After 2 min of polarization under various current densities, all voltage curves relax back to the initial OCV because the short periods of discharge have not changed the electrolyte concentration by much.

Furthermore, spontaneous Li enrichment has also been realized when a feeding solution with a higher Mg/Li ratio is employed (Fig. 4d). Using 0.5 M $MgCl_2$ and 0.3 mM LiCl in the feeding solution (Mg/Li molar ratio = 1,667), Li can be transported to a receiving solution with 10 times higher Li^+ concentration (3 mM LiCl + supporting electrolyte), while still outputting energy. However, the current density is limited to about 10 μA cm^{-2} due to the very low concentration of LiCl in the feeding solution. Higher current density leads to a huge overpotential and a positive cell voltage, which will consume rather than produce energy (Supplementary Fig. 4b). This is probably due to Li^+ depletion near the surface of the LAGP membrane in the feeding solution, as validated previously by simulation[69].

Performance and stability of spontaneous Li extraction

As the major source of Li for industry today, continental brines contain nearly 60% of the identified Li resources on shore. Li concentration in these salt lakes usually ranges from 50 to 1,000 ppm, whereas the concentration of chloride well exceeds 1 mol l^{-1} (35.45 g l^{-1}) in most cases[12,81].

To test the overall performance and long-term stability of the spontaneous Li extraction process, we have used a feeding solution with 0.5 M $MgCl_2$ and 0.03 M LiCl (~200 ppm Li) to represent the typical brines. The amount of Li in 50 ml of the feeding solution (1.5 mmol or 40 mAh) greatly exceeds the available capacity of the Ag electrodes, hence the electrodes need to be repeatedly switched after exhausting their capacity. As discussed above in Fig. 1, this can be achieved with just one pair of electrodes, only requiring washing between each switching. As can be seen from Fig. 5a, the voltage profile of spontaneous Li extraction resembles the voltage curves in galvanostatic discharge of batteries, featured with a plateau and a sudden drop of voltage towards the end. The concentration difference of Cl^- across the membrane will get smaller as more Li is extracted from the feeding to the receiving side. In consequence, the discharge voltage decreases with the increasing number of switching as shown in Fig. 5a. Correspondingly, the energy output from the extraction process also decreases from 0.35 mWh (4.7 Wh mol_{Li}^{-1} or 0.68 Wh g_{Li}^{-1}) in the first cycle to less than 0.02 mWh in the last cycle (Fig. 5b). On average, the energy output from the spontaneous Li extraction process is about 1.6 Wh mol_{Li}^{-1} or 0.24 Wh g_{Li}^{-1}.

Figure 5c shows that the Faradaic efficiency of the extraction process maintains around 100% for over 300 h of continuous operation under 0.1 mA cm^{-2} (15 times of switching). The quantity of extracted Li grows linearly with the amount of charge passed through the device, which also illustrates the stability of this process. The spontaneous

https://doi.org/10.1038/s44221-024-00326-2

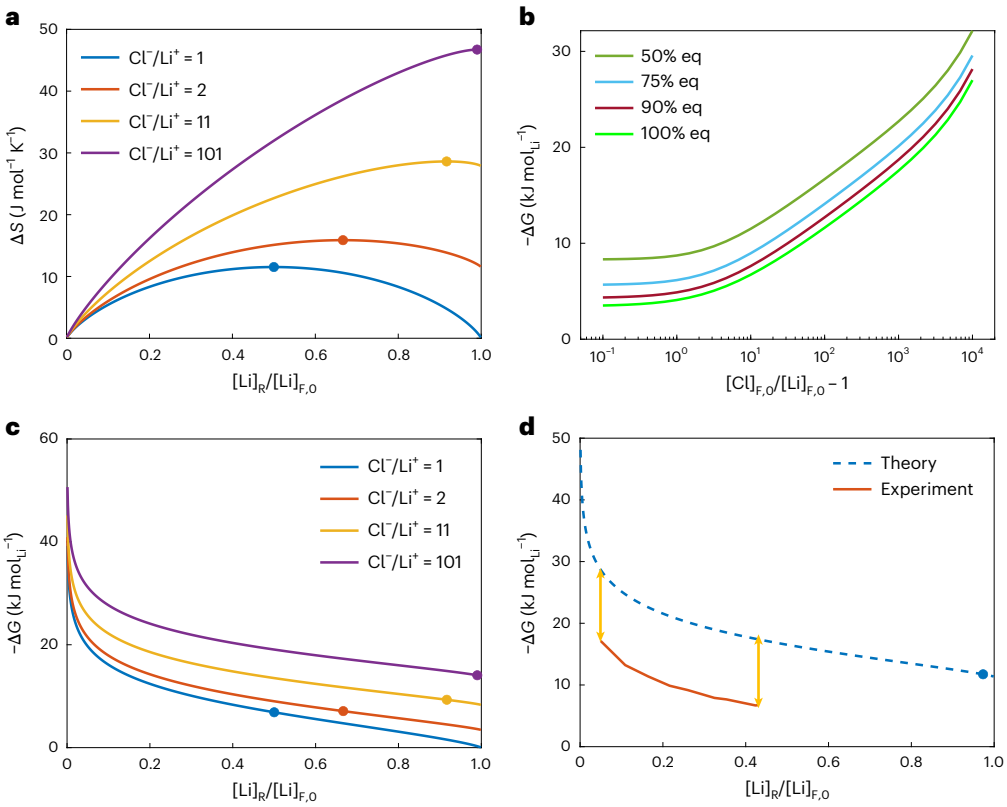

Fig. 6 | Thermodynamic driving force of spontaneous Li extraction processes. a, Molar entropy change of Li extraction as a function of extraction fraction *y*. The lines show Li extraction into pure water from feeding solutions of various ratios between counter ion and Li. The dots indicate the equilibrium position of the system. **b**, Molar Gibbs free energy change of Li extraction as a function of the ratio between counter ion and Li. Different lines represent different cut-off conditions. For example, 50% eq indicates extracting until Li in the receiving solution reaches half of the equilibrium concentration. **c**, Molar Gibbs free energy change of Li extraction as a function of extraction fraction with different ratios between counter ion and Li. **d**, Comparison of experimental results and theoretical prediction of the Molar Gibbs free energy change during Li extraction.

extraction also features a high selectivity thanks to the LAGP membrane, with less than 4% of Mg impurities in the extracted product (Fig. 5d), achieving a Li/Mg molar selectivity of 450. The small amount of Mg crossover has probably been carried to the receiving side by the electrodes during switching, because simple washing is not guaranteed to remove all Mg^{2+} trapped in the porous electrodes.

In theory, the driving force of spontaneous Li extraction comes almost purely from entropy change, which can be calculated using the following formula:

$$\Delta S_{tot} = -RVc_0\left[y\ln\left(\frac{y^2}{(1-y)(\alpha+1-y)}\right) + \ln(1-y) + (\alpha+1)\ln\left(\frac{\alpha+1-y}{\alpha+1}\right)\right] \quad (7)$$

where R is the ideal gas constant, V is the volume of feeding or receiving solution, c_0 (equivalent to $[Li]_{F,0}$) is the initial concentration of Li in the feeding solution, $y = [Li]_R/[Li]_{F,0}$ is the extraction fraction defined as Li concentration in the receiving solution divided by c_0, and $\alpha + 1$ is the ratio between counter ion and Li (hence α is the ratio between co-ion and Li). The detailed derivation is included in Supplementary Note 1.

As shown in Fig. 6a, the equilibrium point corresponds with the maximum value of the entropy change, and it moves towards larger extraction fraction as α increases. The negative value of Gibbs free energy change ($\Delta G = -T\Delta S$) increases with the ratio between counter ion and Li (Fig. 6b), which infers that more useful work can be generated by the Li extraction process. As the extraction fraction moves closer to the equilibrium value, less energy can be produced from the system per unit of Li extracted (Fig. 6b,c). In practice, energy loss due to the internal resistance and electrode overpotential of Li extraction devices decreases the output energy of Li extraction process. The resistance loss is nearly constant because the cell resistance is relatively stable. As a result the energy efficiency drops from 60% to 40% when the extraction fraction increases from 0.1 to 0.4 (Fig. 6d).

Discussion

Compared with other direct lithium extraction methods, our process not only provides a good selectivity and a high rate, but more importantly, it produces energy rather than consuming it. In Fig. 7, the negative energy consumption (net energy production) of spontaneous Li extraction forms a dramatic contrast with all other prototypes reported in previous literature. This work focuses on demonstrating the feasibility of spontaneous extraction, hence there is still plenty of room for performance improvement.

First, the rate of extraction may be further increased by minimizing the cell impedance, increasing the current density and feeding concentration of Li. Reducing the distance between the electrodes, using a thinner membrane with higher ionic conductivity and tuning the structure of the electrodes to reduce overpotential could greatly reduce the total resistance. We have already shown in Fig. 4c that the system could still output energy even when the current density is increased by a factor of 2.5. Some of the highest extraction rates in literature were achieved using feeding solutions with Li concentration greater than 0.5 M (refs. 51,66), showing the large impact of feeding concentration. Second, cheaper and more durable materials for the chloride-storing electrode and membrane might be used to reduce the system cost. BiOCl and layered double hydroxide have been explored

https://doi.org/10.1038/s44221-024-00326-2

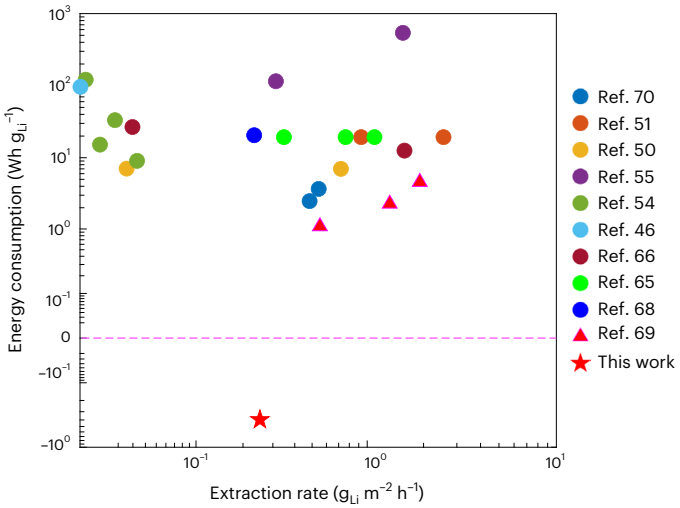

Fig. 7 | Comparison of energy consumption and extraction. Comparison of the energy consumption and extraction rate of spontaneous Li extraction with other direct lithium extraction methods.

as promising candidates for low-cost chloride-storing electrodes[82–89], which could reduce the cost of electrode material by over ten times. The unit cost of the membrane could be decreased by fabricating thinner composite membrane of LAGP and polymer or by employing lower-cost Si-doped LATP[90]. Third, the spontaneous Li extraction process could become more scalable and fully continuous by introducing a stacked device structure similar to reverse electrodialysis. By staking multiple pairs of LAGP and anion exchange membrane, the cell voltage could be high enough to induce a water-splitting reaction so that electrode switching is no longer needed, and the processing capacity could be substantially improved.

Finally, the stability of Li-selective membranes in Na-rich solutions needs to be improved. In addition to Li/Mg separation, Li/Na separation was also performed in this work, which results in similar energy output (Supplementary Fig. 5). However, the device experiences a stability issue over long periods of operation in Na-rich brines. Both Li selectivity and Faradaic efficiency begin to drop continuously after operating for about 40 h in Na brines, and the Li extraction slows down as more impurities are transported (Supplementary Fig. 6a–c). Post-mortem examination reveals that multiple cracks have formed on the LAGP ceramic membrane operated in Na brines, whereas no such defects are formed in Mg brines (Supplementary Fig. 6d). The equilibrium conditions in Li–Na systems also deviate severely from the theory, especially at high Na/Li ratio (Supplementary Fig. 6e). When simply immersed in Na^+-containing solutions, LAGP has been observed to release up to 40% of its Li into the solution (Supplementary Fig. 6f). Using multiple characterization tools, we have confirmed that the Li^+ in LAGP lattice has exchanged with Na^+ from the solution. Due to the larger ionic radii of bare Na^+ ions, such an exchange leads to lattice expansion and stress (Supplementary Figs. 7 and 8), which eventually develop into macroscopic cracks, causing membrane failure. The pH of the receiving solution also plays a role in the stability of the membrane. NH_4HCO_3 (pH 8.6 at 0.1 M) has been chosen over other supporting electrolytes such as $(NH_4)_2SO_4$ (pH 5.6 at 0.06 M), because alkaline solution tends to be less corrosive towards LAGP than acidic solution and results in a higher Faradaic efficiency (Supplementary Fig. 9). This observation is consistent with recent publications, which demonstrated that LAGP can operate stably for more than 40 h even in a strongly alkaline solution of 3 M LiOH[49].

In summary, we introduce the concept of spontaneous ion separation driven by counter-ion gradients. Through both theory and experiments, we have verified that such a mechanism not only can produce energy during Li/Mg separation but also shows potential for spontaneous Li enrichment from brines. Using LAGP as a Li-selective membrane, our prototypic set-up retains a good Li/Mg selectivity of 450 and a near-unity Faradaic efficiency for 300 h of operation, whereas outputting 1.6 Wh mol_{Li}^{-1} of energy. The principle demonstrated in this work paves the way for carbon-negative Li extraction, which has never been thought of. It also opens the gate to a new energy source hidden in ion-separation processes, which could be applied to greatly lower the energy cost of recovering various valuable elements[91,92].

Methods

Preparation of LAGP membrane

LAGP powder was purchased from MSE Supplies LLC. The LAGP powder was pressed in a die set under constant uniaxial pressure of 20 MPa for 1 min. The green pellet was then sintered at 850 °C for 6 h in a tube furnace. The sintered LAGP pellets had a diameter of about 16.0 mm. The pellets were attached onto a circular hole in an acrylic panel using epoxy glue. The exposed area of LAGP is designed as 1 cm^2.

Preparation of Ag and AgCl electrodes

Ag electrodes were prepared by applying silver paste (Silver Print II, 22-023, GC Electronics) onto carbon paper (AvCarb P50) and then drying on a hotplate at 80 °C overnight. The dimension of the electrodes was around 1.5 by 2.5 cm. AgCl electrodes were obtained by electrochemically oxidizing the Ag electrodes in 0.5 M NaCl solution, using pristine carbon paper as the counter electrode. A pair of Ag and AgCl electrodes were then cycled in 0.5 M NaCl solution under 0.16 mA cm^{-2} current density for five cycles before being used for Li extraction. The mass loading of Ag paste was about 0.01 g cm^{-2} and the available capacity was about 2.5 mAh.

Material characterization

The crystalline structure of LAGP membranes was analysed by X-ray diffraction (XRD; PANalytical Empyrean with a Cu(Kα) X-ray source). Diffraction patterns were collected from 10° to 70° using a step size of 0.01°. A scanning electron microscope (SEM; Thermo Fisher Scientific Apreo) was used to investigate the microstructural evolution of LAGP during Li extraction. An energy-dispersive X-ray (EDS) detector (XFlash 6|60 SDD) integrated into the SEM was used to map the elemental distributions. X-ray photoelectron spectroscopy (PHI VersaProbe III with a monochromatized Al(Kα) X-ray source) was used to characterize the change of surface elemental compositions in the LAGP membrane after exposure to brine.

Electrochemical cell assembly and direct Li extraction

The H-shape electrochemical cell was purchased from Adams & Chittenden Scientific Glass. The acrylic panel with LAGP was sandwiched between the two chambers of H cell, sealed with two rubber O-rings and a clamp. Each of the two chambers contains 50 ml of solution and was continuously stirred with a magnetic stirrer. The feeding solution was 0.5 M $MgCl_2$ with various concentrations of LiCl as indicated in the main text. The receiving solution was 0.1 M NH_4HCO_3 unless mentioned otherwise. The Ag and AgCl electrodes were attached onto titanium holder clips and placed into the feeding and receiving chambers, respectively. For the long-term stability test, after the cell was discharged at 0.1 mA for 20 h, the two electrodes would be taken out and washed with deionized water. The two electrodes were then switched and the process was repeated until the discharge capacity was less than 1 mAh with a cut-off voltage of 0 V. Between each switching, 50 µl of the feeding solution and receiving solution were collected and then diluted with a 2% aqueous nitric acid solution for inductively coupled plasma mass spectrometry analysis (Thermo Scientific XSERIES 2 Quadrupole).

The impedance of the cell was determined by the electrochemical impedance spectroscopy (EIS) (Biologic VMP3 system) with a frequency range from 1 MHz to 0.1 Hz and a perturbation voltage of 10 mV

at room temperature. For the OCV and EIS experiments, the composition of the feeding solution was fixed whereas the LiCl content in the receiving solution was ramped up by adding 3 M LiCl solution.

Faradaic efficiency, Li selectivity and energy output

The Faradaic efficiency was calculated by

$$\mathrm{FE} = \frac{ZFV\Delta C_{\mathrm{Li}^+}}{Q}$$

where Z is the charge number of Li ion, F is the Faraday constant, V is the volume of the receiving solution in the cell, ΔC_{Li^+} is the variation of Li ion concentration in the receiving solution and Q is the charge consumption. The nominal Li selectivity was calculated by

$$\text{Li selectivity} = \frac{\Delta C_{\mathrm{Li}^+}}{\left(\Delta C_{\mathrm{Li}^+} + \Delta C_{\mathrm{Mg}^{2+}}\right)}$$

where $\Delta C_{\mathrm{Mg}^{2+}}$ is the variation of Mg-ion concentration in the receiving solution.

The nominal Li selectivity (sometimes called purity in other literature) was used throughout the paper in all figures and would always take a value between 0 and 100%. In comparison, the Li/Mg binary selectivity (or separation factor) of 450 reported in the abstract was defined as:

$$\text{Li/Mg selectivity} = \frac{\Delta C_{\mathrm{Li}^+} / C_{\mathrm{Li}^+,i}}{\Delta C_{\mathrm{Mg}^{2+}} / C_{\mathrm{Mg}^{2+},i}}$$

where $C_{\mathrm{Li}^+,i}$ and $C_{\mathrm{Mg}^{2+},i}$ are the initial concentrations of Li and Mg ions in the feeding solution.

The energy output was calculated by

$$\text{Energy output} = \frac{QU}{V\Delta C_{\mathrm{Li}^+} M_{\mathrm{Li}^+}}$$

where U is the average applied voltage and M_{Li^+} is the molecular weight of Li ions.

Data availability

All data are presented in the article and its Supplementary Information.

References

1. Greim, P., Solomon, A. A. & Breyer, C. Assessment of lithium criticality in the global energy transition and addressing policy gaps in transportation. *Nat. Commun.* **11**, 4570 (2020).
2. Degen, F., Winter, M., Bendig, D. & Tübke, J. Energy consumption of current and future production of lithium-ion and post lithium-ion battery cells. *Nat. Energy* **8**, 1284–1295 (2023).
3. Martin, G., Rentsch, L., Höck, M. & Bertau, M. Lithium market research—global supply, future demand and price development. *Energy Storage Mater.* **6**, 171–179 (2017).
4. Kumar, A., Fukuda, H., Hatton, T. A. & Lienhard, J. H. V. Lithium recovery from oil and gas produced water: a need for a growing energy industry. *ACS Energy Lett.* **4**, 1471–1474 (2019).
5. Song, J. F., Nghiem, L. D., Li, X.-M. & He, T. Lithium extraction from Chinese salt-lake brines: opportunities, challenges, and future outlook. *Environ. Sci. Water Res. Technol.* **3**, 593–597 (2017).
6. Meshram, P., Pandey, B. D. & Mankhand, T. R. Extraction of lithium from primary and secondary sources by pre-treatment, leaching and separation: a comprehensive review. *Hydrometallurgy* **150**, 192–208 (2014).
7. Zhang, Y., Hu, Y., Wang, L. & Sun, W. Systematic review of lithium extraction from salt-lake brines via precipitation approaches. *Miner. Eng.* **139**, 105868 (2019).
8. DuChanois, R. M. et al. Prospects of metal recovery from wastewater and brine. *Nat. Water* **1**, 37–46 (2023).
9. Zhang, S. et al. Solar-driven membrane separation for direct lithium extraction from artificial salt-lake brine. *Nat. Commun.* **15**, 238 (2024).
10. Chen, X. et al. Spatially separated crystallization for selective lithium extraction from saline water. *Nat. Water* **1**, 808–817 (2023).
11. Li, H.-N. et al. Design of photothermal 'ion pumps' for achieving energy-efficient, augmented, and durable lithium extraction from seawater. *ACS Nano* **18**, 2434–2445 (2024).
12. Vera, M. L., Torres, W. R., Galli, C. I., Chagnes, A. & Flexer, V. Environmental impact of direct lithium extraction from brines. *Nat. Rev. Earth Environ.* **4**, 149–165 (2023).
13. Stringfellow, W. T. & Dobson, P. F. Technology for the recovery of lithium from geothermal brines. *Energies* **14**, 6805 (2021).
14. Liu, Y., Ma, B., Lü, Y., Wang, C. & Chen, Y. A review of lithium extraction from natural resources. *Int. J. Miner. Metall. Mater.* **30**, 209–224 (2022).
15. Mends, E. A. & Chu, P. Lithium extraction from unconventional aqueous resources—a review on recent technological development for seawater and geothermal brines. *J. Environ. Chem. Eng.* **11**, 110710 (2023).
16. Battistel, A., Palagonia, M. S., Brogioli, D., La Mantia, F. & Trocoli, R. Electrochemical methods for lithium recovery: a comprehensive and critical review. *Adv. Mater.* **32**, e1905440 (2020).
17. Zavahir, S. et al. A review on lithium recovery using electrochemical capturing systems. *Desalination* **500**, 114883 (2021).
18. Luo, G., Li, X., Chen, L., Chao, Y. & Zhu, W. Electrochemical lithium ion pumps for lithium recovery: a systematic review and influencing factors analysis. *Desalination* **548**, 116228 (2023).
19. Xiong, Y. et al. Electrochemical lithium extraction from aqueous sources. *Matter* **5**, 1760–1791 (2022).
20. Hill, G. T., Shi, F., Zhou, H., Han, Y. & Liu, C. Layer spacing gradient $(NaLi)_{1-x}CoO_2$ for electrochemical Li extraction. *Matter* **4**, 1611–1624 (2021).
21. Liu, C. et al. Lithium extraction from seawater through pulsed electrochemical intercalation. *Joule* **4**, 1459–1469 (2020).
22. Yan, G. et al. The role of solid solutions in iron phosphate-based electrodes for selective electrochemical lithium extraction. *Nat. Commun.* **13**, 4579 (2022).
23. Yan, G., Wang, M., Hill, G. T., Zou, S. & Liu, C. Defining the challenges of Li extraction with olivine host: the roles of competitor and spectator ions. *Proc. Natl Acad. Sci. USA* **119**, e2200751119 (2022).
24. Xu, W., He, L. & Zhao, Z. Lithium extraction from high Mg/Li brine via electrochemical intercalation/de-intercalation system using $LiMn_2O_4$ materials. *Desalination* **503**, 114935 (2021).
25. Zhao, M.-Y. et al. Study on lithium extraction from brines based on $LiMn_2O_4/Li_{1-x}Mn_2O_4$ by electrochemical method. *Electrochim. Acta* **252**, 350–361 (2017).
26. Marchini, F., Rubi, D., del Pozo, M., Williams, F. J. & Calvo, E. J. Surface chemistry and lithium-ion exchange in $LiMn_2O_4$ for the electrochemical selective extraction of LiCl from natural salt lake brines. *J. Phys. Chem. C* **120**, 15875–15883 (2016).
27. Razmjou, A., Asadnia, M., Hosseini, E., Habibnejad Korayem, A. & Chen, V. Design principles of ion selective nanostructured membranes for the extraction of lithium ions. *Nat. Commun.* **10**, 5793 (2019).
28. Hou, J. et al. Lithium extraction by emerging metal–organic framework-based membranes. *Adv. Funct. Mater.* **31**, 2105991 (2021).
29. Wen, Q. et al. Highly selective ionic transport through subnanometer pores in polymer films. *Adv. Funct. Mater.* **26**, 5796–5803 (2016).

30. Lu, Z., Wu, Y., Ding, L., Wei, Y. & Wang, H. A lamellar MXene ($Ti_3C_2T_x$)/PSS composite membrane for fast and selective lithium-ion separation. *Angew. Chem. Int. Ed.* **60**, 22265–22269 (2021).
31. Xu, R., Kang, Y., Zhang, W., Zhang, X. & Pan, B. Oriented UiO-67 metal-organic framework membrane with fast and selective lithium-ion transport. *Angew. Chem. Int. Ed.* **61**, e202115443 (2022).
32. Ruan, X. et al. Constructing mechanical shuttles in a three-dimensional (3D) porous architecture for selective transport of lithium ions. *Angew. Chem. Int. Ed.* **62**, e202216549 (2023).
33. Paredes, C. & Rodríguez de San Miguel, E. Selective lithium extraction and concentration from diluted alkaline aqueous media by a polymer inclusion membrane and application to seawater. *Desalination* **487**, 114500 (2020).
34. Tong, X. et al. MXene composite membranes with enhanced ion transport and regulated ion selectivity. *Environ. Sci. Technol.* **56**, 8964–8974 (2022).
35. Pang, S. et al. 2D nanofluidic vermiculite membranes with self-confinement channels and recognition sites for ultrafast lithium ion-selective transport. *J. Membr. Sci.* **687**, 122054 (2023).
36. Xin, W. et al. Nacre-like mechanically robust heterojunction for lithium-ion extraction. *Matter* **4**, 737–754 (2021).
37. Lu, Y. et al. Engineer nanoscale defects into selective channels: MOF-enhanced Li^+ separation by porous layered double hydroxide membrane. *Nano-Micro Lett.* **15**, 147 (2023).
38. Warnock, S. J. et al. Engineering Li/Na selectivity in 12-crown-4-functionalized polymer membranes. *Proc. Natl Acad. Sci. USA* **118**, e2022197118 (2021).
39. Chang, W. J. et al. MoS_2 passivated multilayer graphene membranes for Li-ion extraction from seawater. *Small* **19**, e2207020 (2023).
40. Wang, R., He, R., He, T., Elimelech, M. & Lin, S. Performance metrics for nanofiltration-based selective separation for resource extraction and recovery. *Nat. Water* **1**, 291–300 (2023).
41. Ye, T. et al. Highly selective lithium transport through crown ether pillared angstrom channels. *Angew. Chem. Int. Ed*. https://doi.org/10.1002/anie.202316161 (2024).
42. Peng, H., Liu, X., Su, Y., Li, J. & Zhao, Q. Advanced lithium extraction membranes derived from tagged-modification of polyamide networks. *Angew. Chem. Int. Ed.* **62**, e202312795 (2023).
43. Peng, H. et al. Quaternization-spiro design of chlorine-resistant and high-permeance lithium separation membranes. *Nat. Commun.* **14**, 5483 (2023).
44. Lu, J. et al. Efficient metal ion sieving in rectifying subnanochannels enabled by metal-organic frameworks. *Nat. Mater.* **19**, 767–774 (2020).
45. Tan, R. et al. Hydrophilic microporous membranes for selective ion separation and flow-battery energy storage. *Nat. Mater.* **19**, 195–202 (2020).
46. Kunugi, S., Inaguma, Y. & Itoh, M. Electrochemical recovery and isotope separation of lithium ion employing lithium ion conductive perovskite-type oxides. *Solid State Ionics* **122**, 35–39 (1999).
47. Hu, J. et al. A lithium feedstock pathway: coupled electrochemical extraction and direct battery materials manufacturing. *ACS Energy Lett.* **7**, 2420–2427 (2022).
48. Fu, L. et al. Electrochemical ion-pumping-assisted transfer system featuring a heterogeneous membrane for lithium recovery. *Chem. Eng. J.* **435**, 134955 (2022).
49. Jiang, Z. et al. $Li_{1.5}Al_{0.5}Ge_{1.5}(PO_4)_3$ membrane electrodialysis for lithium enrichment. *J. Membr. Sci.* **670**, 121353 (2023).
50. Huang, H. et al. Photoelectrochemical lithium extraction. *Nano Energy* **115**, 108683 (2023).
51. Fu, L. et al. Engineering multi-field-coupled synergistic ion transport system based on the heterogeneous nanofluidic membrane for high-efficient lithium extraction. *Nano Micro Lett.* **15**, 130 (2023).
52. Li, Z. et al. Green lithium: photoelectrochemical extraction. *PhotoniX* **4**, 23 (2023).
53. Ounissi, T., Dammak, L., Larchet, C., Fauvarque, J. F. & Selmane Bel Hadj Hmida, E. Novel lithium selective composite membranes: synthesis, characterization and validation tests in dialysis. *J. Mater. Sci.* **55**, 16111–16128 (2020).
54. Shen, K. et al. Flexible LATP composite membrane for lithium extraction from seawater via an electrochemical route. *J. Membr. Sci.* **671**, 121358 (2023).
55. Ounissi, T. et al. Lithium-sodium separation by a lithium composite membrane used in electrodialysis process: concept validation. *Membranes* **12**, 244 (2022).
56. Ounissi, T., Dammak, L., Fauvarque, J. F. & Selmane Bel Hadj Hmida, E. Ecofriendly lithium-sodium separation by diffusion processes using lithium composite membrane. *Sep. Purif. Technol.* **275**, 119134 (2021).
57. Mashtalir, O., Nguyen, M., Bodoin, E., Swonger, L. & O'Brien, S. P. High-purity lithium metal films from aqueous mineral solutions. *ACS Omega* **3**, 181–187 (2018).
58. Zhang, F. et al. A low-cost anodic catalyst of transition metal oxides for lithium extraction from seawater. *Chem. Commun.* **56**, 6396–6399 (2020).
59. Zhao, X., Zhang, H., Yuan, Y., Ren, Y. & Wang, N. Ultra-fast and stable extraction of Li metal from seawater. *Chem. Commun.* **56**, 1577–1580 (2020).
60. Wu, X. et al. Highly efficient and stable Li extraction device by coupling $Li_4Ti_5O_{12}$ electrode and matching perfluoro electrolyte. *J. Alloys Compd.* **869**, 159402 (2021).
61. Yang, S., Zhang, F., Ding, H., He, P. & Zhou, H. Lithium metal extraction from seawater. *Joule* **2**, 1648–1651 (2018).
62. Zhang, H., Ren, Y., Wu, X. & Wang, N. An interface-modified solid-state electrochemical device for lithium extraction from seawater. *J. Power Sources* **482**, 228938 (2021).
63. Lang, J. et al. High-purity electrolytic lithium obtained from low-purity sources using solid electrolyte. *Nat. Sustain.* **3**, 386–390 (2020).
64. Hoshino, T. Innovative lithium recovery technique from seawater by using world-first dialysis with a lithium ionic superconductor. *Desalination* **359**, 59–63 (2015).
65. Morita, K., Matsumoto, T. & Hoshino, T. Efficient lithium extraction via electrodialysis using acid-processed lithium-adsorbing lithium lanthanum titanate. *Desalination* **543**, 116117 (2022).
66. Li, Z. et al. Continuous electrical pumping membrane process for seawater lithium mining. *Energy Environ. Sci.* **14**, 3152–3159 (2021).
67. Sasaki, K., Hiraka, R., Takahashi, H. & Shin-mura, K. Energy balance of lithium recovery by electrodialysis using $La_{0.57}Li_{0.29}TiO_3$ electrolyte. *Fusion Eng. Des.* **170**, 112500 (2021).
68. Hoshino, T. Recycling of used Li-ion batteries by innovative electrodialysis using new lithium ionic conductor membrane. *ECS Meeting Abstr.* **MA2019-02**, 1021 (2019).
69. Xu, R. et al. Continuous lithium extraction from brine by efficient redox-couple electrodialysis. *Matter* https://doi.org/10.1016/j.matt.2024.07.014 (2024).
70. Wang, L. et al. Redox flow battery for continuous and energy-effective lithium recovery from aqueous solution. *ACS Energy Lett.* **7**, 3539–3544 (2022).
71. Donnan, F. G. The theory of membrane equilibria. *Chem. Rev.* **1**, 73–90 (1924).
72. He, K. et al. Stability of lithium ion conductor NASICON structure glass ceramic in acid and alkaline aqueous solution. *Solid State Ionics* **254**, 78–81 (2014).

73. Kallay, N., Preocanin, T. & Supljika, H. Measurement of surface potential at silver chloride aqueous interface with single-crystal AgCl electrode. *J. Colloid Interface Sci.* **327**, 384–387 (2008).
74. Mariappan, C. R., Yada, C., Rosciano, F. & Roling, B. Correlation between micro-structural properties and ionic conductivity of $Li_{1.5}Al_{0.5}Ge_{1.5}(PO_4)_3$ ceramics. *J. Power Sources* **196**, 6456–6464 (2011).
75. Zhang, M. H. et al. Research on Li^+/Na^+ selectivity of NASICON-type solid-state ion conductors by first-principles calculations. *Energy Fuels* **37**, 10663–10672 (2023).
76. Weiss, M., Weber, D. A., Senyshyn, A., Janek, J. & Zeier, W. G. Correlating transport and structural properties in $Li_{1+x}Al_xGe_{2-x}(PO_4)_3$ (LAGP) prepared from aqueous solution. *ACS Appl. Mater. Interfaces* **10**, 10935–10944 (2018).
77. Dove, P. M. & Nix, C. J. The influence of the alkaline earth cations, magnesium, calcium, and barium on the dissolution kinetics of quartz. *Geochim. Cosmochim. Acta* **61**, 3329–3340 (1997).
78. Schmid, R., Miah, A. M. & Sapunov, V. N. A new table of the thermodynamic quantities of ionic hydration: values and some applications (enthalpy-entropy compensation and Born radii). *Phys. Chem. Chem. Phys.* **2**, 97–102 (2000).
79. Ha, H. & Payer, J. The effect of silver chloride formation on the kinetics of silver dissolution in chloride solution. *Electrochim. Acta* **56**, 2781–2791 (2011).
80. Katan, T., Szpak, S. & Bennion, D. N. Silver/silver chloride electrodes: surface morphology on charging and discharging. *J. Electrochem. Soc.* **121**, 757–764 (1974).
81. Sun, Y., Wang, Q., Wang, Y., Yun, R. & Xiang, X. Recent advances in magnesium/lithium separation and lithium extraction technologies from salt lake brine. *Sep. Purif. Technol.* **256**, 117807 (2021).
82. Wang, K. et al. Chloride pre-intercalated CoFe-layered double hydroxide as chloride ion capturing electrode for capacitive deionization. *Chem. Eng. J.* **433**, 133578 (2022).
83. Dou, Q. et al. Emerging trends in anion storage materials for the capacitive and hybrid energy storage and beyond. *Chem. Soc. Rev.* **50**, 6734–6789 (2021).
84. Liu, Q. et al. Rechargeable anion-shuttle batteries for low-cost energy storage. *Chem* **7**, 1993–2021 (2021).
85. Chen, F. et al. Dual-ions electrochemical deionization: a desalination generator. *Energy Environ. Sci.* **10**, 2081–2089 (2017).
86. Chen, F., Leong, Z. Y. & Yang, H. Y. An aqueous rechargeable chloride ion battery. *Energy Storage Mater.* **7**, 189–194 (2017).
87. Nam, D. H. & Choi, K. S. Bismuth as a new chloride-storage electrode enabling the construction of a practical high capacity desalination battery. *J. Am. Chem. Soc.* **139**, 11055–11063 (2017).
88. Huang, Z. et al. Anion chemistry in energy storage devices. *Nat. Rev. Chem.* **7**, 616–631 (2023).
89. Liang, G., Mo, F., Ji, X. & Zhi, C. Non-metallic charge carriers for aqueous batteries. *Nat. Rev. Mater.* **6**, 109–123 (2020).
90. Chang, B. et al. Low-cost and stable $Li_{1.5}Al_{0.3}Ti_{1.7}Si_{0.2}P_{2.8}O_{12}$ glass–ceramics for lithium extraction from seawater. *J. Solid State Electrochem.* https://doi.org/10.1007/s10008-024-06015-0 (2024).
91. Liu, C. et al. A half-wave rectified alternating current electrochemical method for uranium extraction from seawater. *Nat. Energy* **2**, 17007 (2017).
92. Ye, Y. et al. Spontaneous electrochemical uranium extraction from wastewater with net electrical energy production. *Nat. Water* **1**, 887–898 (2023).

Acknowledgements

Part of this work was performed at the Stanford Nano Shared Facilities (SNSF), supported by the National Science Foundation under award ECCS-2026822. Part of this work was performed in the nano@Stanford labs, supported by the National Science Foundation as part of the National Nanotechnology Coordinated Infrastructure under award ECCS-1542152. This work was supported by the Stanford StorageX Initative.

Author contributions

G.Z. conceived the idea. G.Z., R.X., X. Xiao and S.B.S. conducted the sample fabrication and processing. G.Z., Y.L., X.G. and G.F. performed the material characterizations. G.Z., H.S., G.H. and X. Xu performed the electrochemical test and data analysis. G.Z., S.C.K., J.Z. and A.W. analysed the theoretical mechanism. G.Z. and Y.C. wrote and revised the paper. All authors contributed to the discussion of the paper.

Competing interests

The authors declare no competing interests.

Additional information

Supplementary information The online version contains supplementary material available at https://doi.org/10.1038/s44221-024-00326-2.

Correspondence and requests for materials should be addressed to Yi Cui.

Peer review information *Nature Water* thanks Yongsheng Chen and Lu Shao for their contribution to the peer review of this work.